# Improvement of photoemission performance of a gradient-doping transmission-mode GaAs photocathode*

Zhang Yi-Jun(张益军), Niu Jun(牛 军), Zhao Jing(赵 静), Xiong Ya-Juan(熊雅娟), Ren Ling(任 玲), Chang Ben-Kang(常本康)†, and Qian Yun-Sheng(钱芸生)

*Institute of Electronic Engineering and Optoelectronic Technology, Nanjing University of Science and Technology, Nanjing* 210094, *China*

(Received 12 April 2011; revised manuscript received 22 August 2011)

Two types of transmission-mode GaAs photocathodes grown by molecular beam epitaxy are compared in terms of activation process and spectral response, one has a gradient-doping structure and the other has a uniform-doping structure. The experimental results show that the gradient-doping photocathode can obtain a higher photoemission capability than the uniform-doping one. As a result of the downward graded band-bending structure, the cathode performance parameters, such as the electron average diffusion length and the surface electron escape probability obtained by fitting quantum yield curves, are greater for the gradient-doping photocathode. The electron diffusion length is within a range of from 2.0 to 5.4 μm for doping concentration varying from $10^{19}$ to $10^{18}$ $cm^{-3}$ and the electron average diffusion length of the gradient-doping photocathode achieves 3.2 μm.

**Keywords:** transmission-mode photocathode, gradient-doping, Cs–O activation, quantum yield

**PACS:** 85.60.Ha, 73.61.Ey, 73.20.At, 79.60.–i **DOI:** 10.1088/1674-1056/20/11/118501

## 1. Introduction

Negative electron affinity (NEA) GaAs photocathodes achieved by the coadsorption of cesium and oxygen have widespread applications in vacuum detecting devices and polarized electron sources because of their virtues of high quantum efficiency, low dark emission and narrow energy spread.[1−5] Currently, the state-of-the-art image intensifiers used for night vision goggles are based on the transmission-mode (t-mode) GaAlAs/GaAs photocathode, which is treated as the key component in the photon–electron conversion process.[2,4] The overall t-mode cathode performance depends mainly on three factors, namely electron diffusion length, back interface recombination velocity and surface electron escape probability, which are related to the material quality and preparation process. In view of this case, many investigations have been performed to improve cathode performance through the progress of epitaxial growth technique and the optimization of activation craft.[6−9]

In the research of polarized electron sources, a gradient-doping structure has been successfully applied to the GaAs strained photocathode, which increases the polarization approaching 80% by overcoming the surface charge limit.[10,11] However, this gradient-doping structure is at the expense of quantum efficiency in which a very thin GaAs surfacelayer with a higher p-type doping concentration on the top of the bulk activelayer in turn prevents more photoelectrons from escaping across surface barrier into vacuum. Therefore, with an attempt to increase electron emission efficiency of NEA photocathodes, the gradient-doping structure for operation in night vision imaging detection should be different. In this paper, another gradient-doping structure with the doping concentration distributed from high to low in the bulk-to-surface GaAs active-layer, which has been proved by our reflection-mode (r-mode) cathode activation experiments,[12,13] is employed to the t-mode GaAs photocathode. To investigate the improvement of cathode photoemission performance, we analyse the variation in band bending structure arising from the gradient-doping structure and compare the difference in photoemission behaviour, namely the activation process and spectral response under the same preparation condition, between the gradient-doping and the uniform-doping t-mode GaAs photocathodes.

*Project supported by the National Natural Science Foundation of China (Grant Nos. 60801036 and 61067001), the Key Science and Technology Project of Henan Province of China (Grant No. 112102210202), and the Research and Innovation Plan for Graduate Students of Jiangsu Higher Education Institutions of China (Grant No. CX09B_096Z).

†Corresponding author. E-mail: bkchang@mail.njust.edu.cn

© 2011 Chinese Physical Society and IOP Publishing Ltd

## 2. Experiment

In order to determine the effect of gradient-doping structure on cathode performance, two different types of t-mode GaAlAs/GaAs photocathode samples were designed, in which one has a gradient-doping structure and the other has a uniform-doping structure. The parameters including the thickness and doping levels of the two samples are shown in Fig. 1, where the stop-layer and cap-layer served as an etch-resistant stopping layer and an inside-oxidation-preventing layer respectively. Their difference is that the GaAs active-layer of 2 μm in total thickness for the gradient-doping sample is divided into four sections with the p-type doping concentration varying from $1 \times 10^{19}$ to $1 \times 10^{18}$ cm$^{-3}$ from bulk to surface, while for the uniform-doping sample, the appropriate doping concentration of GaAs active-layer is $1 \times 10^{19}$ cm$^{-3}$, which is a tradeoff between electron diffusion length and surface electron escape probability.[14] In the two structures, the Al mole fraction and the doping concentration of the GaAlAs window-layer are designed to be 0.63 and $1 \times 10^{19}$ cm$^{-3}$.

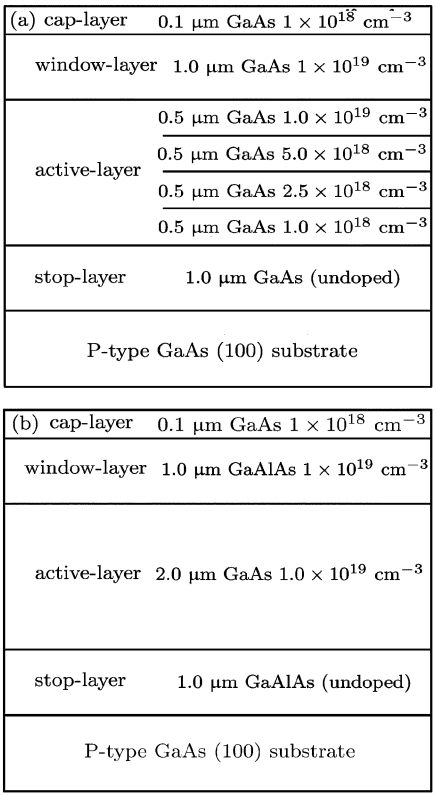



**Fig. 1.** Doping structures of (a) gradient-doping sample and (b) uniform-doping sample grown by MBE.

With the advantage of the molecular beam epitaxy (MBE) technique, which is more suited for the growth of multi-layer structure with an abrupt interface characteristic, the t-mode GaAs photocathode samples with p-type beryllium (Be) doping were grown on a high-quality p-type GaAs (100) oriented substrate by using an Applied EPI Gen-II MBE system. The epitaxial layers with 2-inch in diameter composed of a stop-layer, an active-layer, a window-layer and a cap-layer were grown according to priority. In the whole growth process, the substrate temperatures were held at 580 °C and 600 °C for growing GaAs and GaAlAs under rich arsenic circumstance respectively. The growth rates of GaAs and GaAlAs both were about 1 μm/h, and the crystalline qualities of the epilayers were monitored during growth via reflection high-energy electron diffraction in situ.

After growth, as the process of fabricating t-mode GaAs photocathodes proposed by Antypas *et al.*,[15] the multi-epitaxial layer was made into the cathode module with a glass/$Si_3N_4$/GaAlAs/GaAs structure after selectively etching the GaAs cap-layer, the substrate and the GaAlAs stop-laye. Following the chemical cleaning and heat treatment in vacuum, the Cs–O activation lowering the surface electron affinity to NEA state for the 18-mm-diameter cathode module was performed in an ultrahigh vacuum chamber with the base pressure less than $10^{-9}$ Pa. During the Cs–O activation, we used the improved codeposition activation technique,[3,5] in which a cesium source was continuously supplied but an oxygen source was introduced periodically. For both samples, the Cs/O flux ratios were kept at the same value of 1.65/1.75. After the usual "high–low temperature" two-step activation,[16] the cathode module was transferred from the activation chamber to the sealed vacuum chamber and indium was sealed into a vacuum image tube, in which the microchannel plate (MCP) and fluorescence screen were removed. Finally, the spectral response of the sealed image tube after being transferred into ambient air was measured by the spectral response measurement system.[17]

## 3. Results and discussion

### 3.1. Gradient band structure

With the aid of the Bio-Rad electrochemical capacitance-voltage (ECV) system, the vertical distribution of carrier concentration versus depth in Be-doped GaAlAs/GaAs epilayers after the MBE growth was measured as shown in Fig. 2. An ideal varied-

doping structure of a good many sublayers can be achieved with the MBE growth technique and the measured carrier concentration $N_A$ in the gradient-doping GaAs active-layer ranges from $4 \times 10^{18}$ cm$^{-3}$ to $7 \times 10^{17}$ cm$^{-3}$, which is composed of four sections, while that in the GaAlAs window-layer is less than $3 \times 10^{18}$ cm$^{-3}$. As a result of the partial ionization mechanism,[18] the carrier concentration representing the active dopant concentration is somewhat lower than the actual doping concentration in the active-layer.

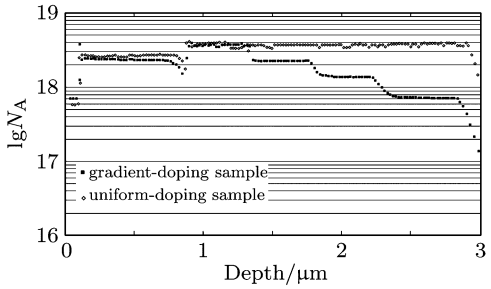



**Fig. 2.** ECV profiles of carrier concentration in the two different samples grown by MBE.

This gradient-doping structure with doping concentration from high to low in the bulk-to-surface GaAs active-layer can result in many downward band bending regions, which help form built-in electric fields to facilitate photoexcited electrons moving toward surface. There is a band-bending region at each interface formed by the Fermi-level leveling effect between two different doping concentration sections. Suppose that the actual carrier concentrations of the two adjacent sections are $N_{A1}$ and $N_{A2}$ respectively, where $N_{A1} > N_{A2}$, the band-bending energy $qV_D$ due to the carrier concentration discrepancy is given by

$$\begin{aligned} qV_D &= E_{F2} - E_{F1} \\ &= \left(E_V + k_0 T \ln \frac{N_V}{N_{A2}}\right) - \left(E_V + k_0 T \ln \frac{N_V}{N_{A1}}\right) \\ &= k_0 T \ln \frac{N_{A1}}{N_{A2}}, \end{aligned} \tag{1}$$

where $E_{F1}$ is the Fermi level of section 1, $E_{F2}$ is the Fermi level of section 2, $k_0$ is Boltzmann constant, $T$ is the absolute temperature, $E_V$ is the valence band maximum and $N_V$ is the valence band density of states of GaAs. Besides, the band bending width $X_D$ in the depletion region of the isotype heterointerface is expressed as

$$X_D = \left[V_D \left(\frac{2\varepsilon_r \varepsilon_0}{q}\right)\left(\frac{N_{A1} + N_{A2}}{N_{A1} N_{A2}}\right)\right]^{1/2}, \tag{2}$$

where $\varepsilon_r$ is the relative permittivity of GaAs material, $\varepsilon_0$ is the vacuum permittivity and $q$ is the electric charge. According to Eqs. (1) and (2), the band-bending energy and width of the gradient-doping GaAs active-layer composed of four sections after the MBE growth are obtained, which are listed in Table 1. In the GaAs active-layer, section 1 corresponds to the layer with the highest carrier concentration while section 4 corresponds to the layer with the lowest carrier concentration. Usually, the surface state tends to pin the Fermi level at about 1/3 bandgap energy ($E_g$) above the valence band maximum, which is responsible for the surface band bending.[19] The width of the resulting surface band-bending region (BBR) can be calculated according to the following expression:

$$d_S = \left(\frac{2\varepsilon_r \varepsilon_0 V_S}{q N_{AS}}\right)^{1/2}, \tag{3}$$

where $V_S$ is the amount of surface band bending and $N_{AS}$ is the surface acceptor doping concentration. The electric field intensity of each band-bending area is calculated as listed in Table 1, which is powerful enough to effectively improve the photoexcited electrons moving toward surface.

Based on the above analysis of the band-bending in the gradient-doping GaAs active-layer, a downward gradient band structure from the GaAs bulk to the surface is formed in the gradient-doping t-mode photocathodes, which is shown in Fig. 3. It is seen from Fig. 3 that for the gradient-doping t-mode photocathodes, most of the photoexcited electrons which suffer energy loss and relax into the Γ conduction-band minimum can obtain extra energy

**Table 1.** Band-bending distribution in the gradient-doping GaAs sample grown by MBE.

| Position | Band-bending energy/meV | Band-bending width/nm | Electric field intensity/kV·cm$^{-1}$ |
|---|---|---|---|
| Section 1–Section 2 | 16.7 | 4.2 | 39.8 |
| Section 2–Section 3 | 10.5 | 4.3 | 24.4 |
| Section 3–Section 4 | 18.0 | 7.5 | 24.0 |
| Surface BBR | 500 | 32.2 | 155.3 |

prior to emission due to the built-in electric fields formed by the downward gradient band structure. It is useful to make the photoexcited electrons moving toward surface speed up in a way of both diffusion and directional drift under the built-in electric fields. Therefore, the electron emission efficiency in gradient-doping GaAs photocathodes can be improved in contrast with that in uniform-doping ones.

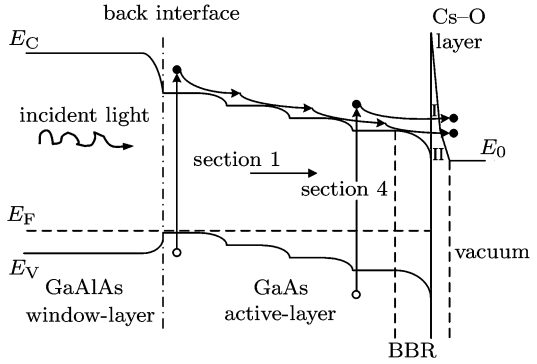



**Fig. 3.** Band structure diagram of the gradient-doping t-mode GaAs photocathode. $E_C$ is the conduction band minimum, $E_V$ is the valence band maximum, $E_g$ is the band gap, $E_F$ is the Fermi level, $E_0$ is the vacuum level and BBR is the surface band-bending region.

## 3.2. Cs–O activation process

The entire Cs–O activation process comprises two stages, which are called stage I and stage II, corresponding to the initial Cs activation and the Cs–O alternate activation. During the two stages, there is a very interesting phenomenon that no matter whether in high-temperature activation or in low-temperature activation, the photocurrent peak of the gradient-doping GaAs sample during the initial stage of Cs exposure activation is smaller and the time for the initial exposure to Cs is longer than that of the uniform-doping one. Figure 4 shows the photocurrent evolutions of the two samples during the initial stage of Cs activation and the Cs–O alternate activation in high-temperature activation respectively. It is evident that the photocurrent for the uniform-doping sample increases faster and the peak value is higher in the initial Cs–O activation process. However, with the increase of activation time, the gradient-doping sample gradually exceeds the uniform-doping one in the photocurrent peak during the subsequent Cs–O activation cycles.

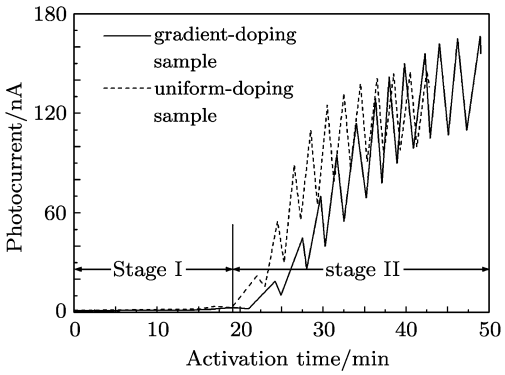



**Fig. 4.** Photocurrent evolutions of the two different samples during the Cs–O activation.

Prior to emission into vacuum, photoexcited electrons must travel across the surface potential barrier, which is related to the Cs–O activation layer. As shown in Fig. 3, the surface potential barrier profile based on the double dipole model comprises two approximately straight lines with different slopes, namely potential barriers I and II.[20] During the initial stage of Cs activation, the adsorption of Cs on cathode surface lowers the surface vacuum level to form zero electron affinity. As a result of the relation between the surface doping concentration and the width of surface BBR, the gradient-doping sample with lower surface doping concentration has a wider band-banding region and consequently a larger loss of electrons in BBR and a possibly lower photocurrent peak in the initial Cs deposition. In addition, it should be noted that the initial Cs deposition causes the reduction of the surface potential barrier I. It is presumed that the first photocurrent maximum is also attributed to the dopinginduced extrinsic surface state and Cs-induced donor state. The Cs atoms become ionic and contribute their valence electrons not only to the dangling bonds but also to the electronegative centres around Be acceptor impurities, then the formed dipole layer named [GaAs (Be)-Cs] acts on the surface state and helps reduce the work function.[21,22] Therefore, on account of the surface doping concentration working on surface BBR and surface states, the resulting disparity in the initial photocurrent peak should be attributed to the surface impurity concentration. The subsequent codepositions of Cs and O, forming the Cs–O dipole layer, would further reduce the work function to achieve the surface NEA state. As a result of the gradient downward band structure in Fig. 3, the potential barrier II for the gradient-doping sample would drop down to a low level relative to the bulk conduction band minimum in comparison with that for the uniform-doping one and more photoelectrons

could escape from cathode surface, which is responsible for the exceeding photocurrent peak obtained by the gradient-doping sample during the succeeding Cs–O activation. In a word, the activation phenomenon suggests that the gradient-doping structure can bring potential photoemission capability to the t-mode photocathodes.

### 3.3. Cathode performance evaluation

The spectral response curves of the two t-mode samples with different structures are shown in Fig. 5. It is clear that the gradient-doping t-mode GaAs photocathode can obtain a higher photosensitivity ranging from 560 nm to 880 nm with an ascending slope. It is noted that especially in the regions of the short-wavelength threshold and the long-wavelength threshold, the gradient-doping photocathode gains a more evident advantage than the uniform-doping one in the photoemission capability. The reason for this phenomenon can be explained by the analysis of the gradient band structure as shown in Fig. 3. For the t-mode photocathodes, the photoelectrons excited by the short-wavelength light in the region near the back interface need to travel a long distance with energy relaxation prior to emission. Owing to the help of the built-in electric fields, there is an obvious virtue that the relaxed electrons in the Γ conduction-band minimum of the gradient-doping photocathode can obtain extra energy and higher emission capability as well. In addition, the electrons with energy close to long-wavelength threshold can still achieve larger escape capability due to the lower surface potential barrier caused by the gradient band structure.

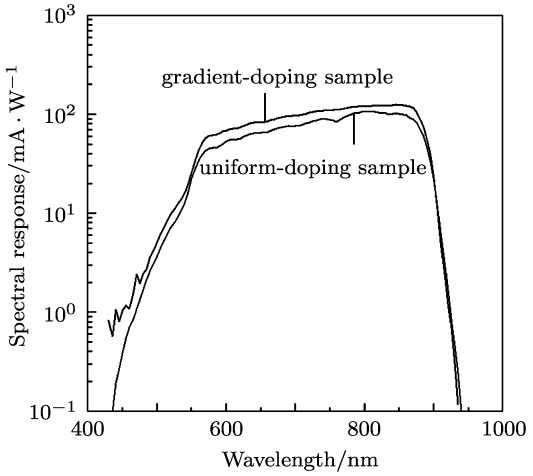



**Fig. 5.** Spectral response curves of the two different samples.

In order to evaluate these intrinsic cathode performance parameters such as electron diffusion length, back interface recombination velocity and surface electron escape probability of the two different t-mode photocathodes, we compare the measured quantum yield curves with the theoretical curves according to the revised quantum yield formula containing the short-wavelength threshold constraint, which is expressed as[4]

$$Y(h\nu) = \frac{P(1-R)\exp(-\beta_{h\nu}T_{\rm w})\alpha_{h\nu}L_{\rm n}}{\alpha_{h\nu}^2L_{\rm n}^2-1}\left\{\frac{\alpha_{h\nu}D_{\rm n}+S_{\rm V}}{(D_{\rm n}/L_{\rm n})\cosh(T_{\rm e}/L_{\rm n})+S_{\rm V}\sinh(T_{\rm e}/L_{\rm n})}\right.$$
$$\left.-\frac{\exp(-\alpha_{h\nu}T_{\rm e})\left[S_{\rm V}\cosh(T_{\rm e}/L_{\rm n})+(D_{\rm n}/L_{\rm n})\sinh(T_{\rm e}/L_{\rm n})\right]}{(D_{\rm n}/L_{\rm n})\cosh(T_{\rm e}/L_{\rm n})+S_{\rm V}\sinh(T_{\rm e}/L_{\rm n})}-\alpha_{h\nu}L_{\rm n}\exp(-\alpha_{h\nu}T_{\rm e})\right\}, \quad (4)$$

where $P$ is the surface electron escape probability, $D_{\rm n}$ is the electron diffusion coefficient, $L_{\rm n}$ is the electron diffusion length, $S_{\rm V}$ is the back interface recombination velocity, $R$ is the reflectivity of photocathode surface, $T_{\rm e}$ is the thickness of the GaAs active-layer, $\alpha_{h\nu}$ is the absorption coefficient of active-layer material, $T_{\rm w}$ is the thickness of the GaAlAs window-layer and $\beta_{h\nu}$ is the absorption coefficient of window-layer material.

As shown in Fig. 6, a good agreement is observed between the theoretical curves and the experimental data for the gradient-doping and uniform-doping samples. By comparing the fitted cathode performance parameters of the two photocathode, we can find that the electron diffusion length and surface electron escape probability of the gradient-doping sample are greater than those of the uniform-doping one. The electron diffusion length of the gradient-doping sample increases due to the lower average doping concentration on the one hand and the increased electron drift length by the aid of electric field traction in the bulk on the other hand. The increase in the surface electron escape probability is because the photoexcited electrons reaching surface BBR could gain additional energy supplied by the induced electric fields in the GaAs bulk. In addition, the surface vacuum level is lower as a result of the gradient band structure and then electrons would turn easy to escape across the surface po-

tential barrier. Therefore, the gradient-doping structure used to prepare the t-mode GaAs photocathodes can not only increase the electron diffusion length but also enhance the electron escape probability.

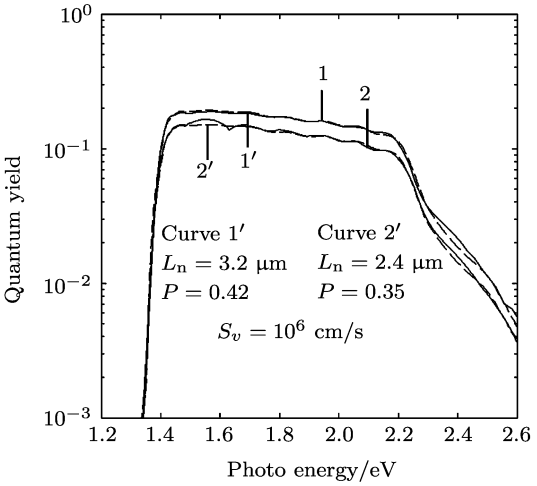



**Fig. 6.** Experimental (solid lines) and theoretical (dashed lines) quantum yield curves. Curves 1 and 1′ represent the results of gradient-doping sample; curves 2 and 2′ denote the results of the uniform-doping sample.

The electron diffusion length of the gradient-doping photocathode inferred through fitting experimental data is essentially the electron average transport length in the active-layer, while the electron diffusion lengths in sections with different doping concentrations from each other can be estimated from $L_n = (D_n\tau_n)^{1/2}$, where the diffusivity $D_n$ is related to the electron mobility $\mu_n$ by the Einstein relation $D_n = k_0T\mu_n/q$. The electronic properties including the minority-carrier mobility ($\mu_n$), the minority-carrier lifetime ($\tau_n$), and the minority-carrier diffusion length ($L_n$) in p-type semiconductor material are important for the analysis of optoelectronic device performance. It is well known that all these electronic properties are inversely proportional to the free-carrier concentration. The minority-carrier mobility in p-type GaAs is significantly lower than the majority-carrier mobility in n-type GaAs at high carrier concentrations and the room-temperature mobility ratio between them is as low as 0.6 for carrier concentration exceeding $10^{18}$ cm$^{-3}$.[23] The value of $\mu_n$ in p-type GaAs of heterojunction bipolar transistor grown by MBE is a function of acceptor carrier concentration at room temperature and is given by[24]

$$\mu_n = \frac{8300}{[1 + N_A/(3.98 \times 10^{15} + N_A/641)]^{1/3}}. \quad (5)$$

Referring to Eq. (5) and the measured carrier concentration by ECV profiling, we can obtain the minority-carrier mobilities in the four sections of gradient-doping GaAs active-layer, as listed in Table 2. As for the minority-carrier lifetime in p-type GaAs, we can only take account of the radiative lifetime which contributes mainly to the overall minority-carrier lifetime for carrier concentration exceeding $10^{18}$ cm$^{-3}$.[25,26] The radiative lifetime can be determined from photoluminescence time-decay measurement, and the empirical formula at room temperature is given by[27]

$$\tau_n = 1/BN_A, \quad (6)$$

where $B$ is the radiative recombination coefficient and is assumed to be $2 \times 10^{-10}$ cm$^3$/s following the previous research.[28,29]

**Table 2.** Electronic properties of the gradient-doping GaAs sample grown by MBE.

| Position | $\mu_n$/cm$^2 \cdot$V$\cdot$s$^{-1}$ | $\tau_n$/ns | $L_n$/μm |
|---|---|---|---|
| Section 1 | 1133 | 1.3 | 2.0 |
| Section 2 | 1253 | 2.4 | 2.8 |
| Section 3 | 1358 | 3.6 | 3.6 |
| Section 4 | 1602 | 7.2 | 5.4 |

According to the obtained minority-carrier mobility and minority-carrier lifetime listed in Table 2, the values of minority-carrier (i.e., electron) diffusion lengths in the four different doping sections are calculated to be in a range from 2.0 to 5.4 μm, which are thought to agree with the calculated results given in Refs. [14] and [30]. Therefore, it is concluded that the increased electron average diffusion length estimated at 3.2 μm in Fig. 6 for the gradient-doping photocathode is realistic and this gradient-doping structure is beneficial to the improvement of photoemission performance.

# 4. Conclusion

A gradient-doping structure is applied to the preparation of t-mode GaAs photocathodes through the MBE technique. The experimental results show that compared with the uniform-doping photocathode, the gradient-doping photocathode exhibits a high photoemission capability in the activation photocurrent and spectral response. In addition, the cathode performance parameters, such as the electron average diffusion length and the electron escape probability obtained by curve fitting according to the revised t-mode quantum yield formula, are increased for the gradient-doping photocathode, which is ascribed to this special varied-doping structure. This work should

be significant to the fabrication of high-performance t-mode III-V NEA photocathodes.

## Acknowledgment

The authors would like to thank Shi Feng, Cheng Hong-Chang, Hu Cang-Lu, Xu Xiao-Bing and Feng Liu at the Key Laboratory of Low Light Level Technology of the Commission of Science Technology and Industry for National Defense for their assistance in the experiment.

## References

[1] Martinelli R U and Fisher D E 1974 *Proc. IEEE* **62** 1339
[2] Estrera J P, Ostromek T, Isbell W and Bacarella A 2003 *Proc. SPIE* **5079** 196
[3] Ruan C J 2003 *Chin. Phys.* **12** 483
[4] Zhang Y J, Niu J, Zhao J, Zou J J and Chang B K 2011 *Acta Phys. Sin.* **60** 067301 (in Chinese)
[5] Zhang Y J, Zou J J, Wang X H, Chang B K, Qian Y S, Zhang J J and Gao P 2011 *Chin. Phys.* B **20** 048501
[6] André J P, Guittard P, Hallais J and Piaget C 1981 *J. Cryst. Growth* **55** 235
[7] Narayanan A A, Fisher D G, Erickson L P and O'Clock G D 1984 *J. Appl. Phys.* **56** 1886
[8] Pastuszka S, Terekhov A S and Wolf A 1996 *Appl. Surf. Sci.* **99** 361
[9] Liu Z, Sun Y, Peterson S and Pianetta P 2008 *Appl. Phys. Lett.* **92** 241107
[10] Maruyama T, Brachmann A, Clendenin J E, Desikan T, Garwin E L, Kirby R E, Luh D A, Turner J and Prepost R 2002 *Nucl. Instrum. Methods Phys. Res.* A **492** 199
[11] Aulenbacher K, Schuler J, Harrach D V, Reichert E, Röthgen J, Subashev A, Tioukine V and Yashin Y 2002 *J. Appl. Phys.* **92** 7536
[12] Zou J J and Chang B K 2006 *Opt. Eng.* **45** 054001
[13] Yang Z, Chang B K, Zou J J, Qiao J L, Gao P, Zeng Y P and Li H 2007 *Appl. Opt.* **46** 7035
[14] Vergara G, Gómez L J, Capmany J and Montojo M T 1997 *Vacuum* **48** 155
[15] Antypas G A, Escher J S, Edgecumbe J and Enck R S 1978 *J. Appl. Phys.* **49** 4301
[16] Stocker B J 1975 *Surf. Sci.* **47** 501
[17] Zhang Y J, Niu J, Zou J J, Chang B K and Xiong Y J 2010 *Appl. Opt.* **49** 3935
[18] Zhang Y J, Chang B K, Yang Z, Niu J, Xiong Y J, Shi F, Guo H and Zeng Y P 2009 *Appl. Opt.* **48** 1715
[19] Gregory P E, Spicer W E, Ciraci S and Harrison W A 1974 *Appl. Phys. Lett.* **25** 511
[20] Su C Y, Spicer W E and Lindau I 1983 *J. Appl. Phys.* **54** 1413
[21] Yang Z, Zou J J, Niu J, Zhang Y J and Chang B K 2010 *Spectrosc. Spect. Anal.* **30** 2038 (in Chinese)
[22] Niu J, Zhang Y J, Chang B K and Xiong Y J 2011 *Acta Phys. Sin.* **60** 044209 (in Chinese)
[23] Walukiewicz W, Lagowski J, Jastrzebski L and Gatos H C 1979 *J. Appl. Phys.* **50** 5040
[24] Tiwari S and Wright S L 1990 *Appl. Phys. Lett.* **56** 563
[25] Casey H C, Miller B I and Pinkas E 1973 *J. Appl. Phys.* **44** 1281
[26] Ito H, Furuta T and Ishibashi T 1991 *Appl. Phys. Lett.* **58** 2936
[27] Casey H C and Stern F 1976 *J. Appl. Phys.* **47** 631
[28] Nelson R J and Sobers R G 1978 *J. Appl. Phys.* **49** 6103
[29] Lovejoy M L, Melloch M R, Lundstrom M S, Keyes B M, Ahrenkiel R K, Lyon T J and Woodall J M 1992 *Appl. Phys. Lett.* **61** 822
[30] Vergara G, Gómez L J, Presa J and Montojo M T 1990 *J. Vac. Sci. Technol.* A **8** 3676